Thermal response of cholesteric liquid crystal elastomers

Hama Nagai and Kenji Urayama*
Department of Macromolecular Science and Engineering, Kyoto Institute of Technology, Matsugasaki, Kyoto 606-8585, Japan
(Received 6 July 2015; published 21 August 2015)

The effects of temperature variation on photonic properties of cholesteric liquid crystal elastomers (CLCEs) are investigated in mechanically unconstrained and constrained geometries. In the unconstrained geometry, cooling in the cholesteric state induces both a considerable shift of the selective reflection band to shorter wavelengths and a finite degree of macroscopic expansion in the two directions normal to the axis of the helical director configuration. The thermal deformation is driven by a change in orientational order of the underlying nematic structure S and the relation between the macroscopic strain and S is explained on the basis of the anisotropic Gaussian chain network model. The helical pitch varies with the film thickness in an affine manner under temperature variation. The CLCEs under the constrained geometry where thermal deformation is strictly prohibited show no shift of the reflection bands when subjected to temperature variation. This also reveals the strong correlation between the macroscopic dimensions and the pitch of the helical director configuration.

DOI: 10.1103/PhysRevE.92.022501 PACS number(s): 61.30.Vx, 61.41.+e, 83.80.Va

I. INTRODUCTION

Liquid crystal elastomers (LCEs) are an intriguing material that has a feature that the macroscopic shape is strongly correlated with molecular orientational order and vice versa [1,2]. This unique feature, which stems from the combination of liquid crystallinity and rubber elasticity, enables us to actuate the LCEs under various types of external stimuli such as temperature variation, electric fields, and light irradiation that affect the molecular orientational order. Among the LCEs with several types of orientational order, cholesteric LCEs (CLCEs) have received much attention as a photonic rubber. Cholesteric LCEs have fascinating photonic properties of cholesteric liquid crystals (CLCs) that originate from the helical director configuration: The CLCs exhibit selective Bragg reflection for incident light with a specific wavelength that is governed by the periodic pitch of the helical configuration [3–5]. The CLCs have potential applications such as reflection displays, tunable lasers, and color reflectors because the selective reflection bands are variable by applying the temperature variation and electric fields. The CLCEs possess the features of CLCs but require no mechanical support for a stable helical configuration of liquid crystals (LCs). Furthermore, the pitch of the helical director configuration, which is coupled to macroscopic dimensions, is tunable by the imposition of mechanical stress (strain) utilizing rubber elasticity [6–12]. The CLCEs are expected to be a promising material for various types of sensors and optical devices.

The response of the CLCEs with monodomain alignment to an external stimulus was first investigated under temperature variation [13]. It was shown that the CLCE films expanded in the directions normal to the helical axis when they were cooled at temperatures below the transition temperature. Bourgerette *et al.* [11] demonstrated that the magnitude of the thermal deformation in the side-chain-type CLCEs depended on the content of odd and even spacer groups. The thermal deformation of the CLCEs is naturally expected to have a correlation with the changes in orientational order of the underlying nematic structure S and the pitch of helical order p_H, but their correlations have not yet been elucidated. The position and width of the selective reflection bands reflect p_H and S, but the temperature dependence of the reflection spectra in CLCEs was not investigated in detail in the earlier studies. Maxein *et al.* [14] reported that the position of the reflection notch in the cross-linked CLC polymer films was unaltered by temperature variation, whereas that in the un-cross-linked ones depended considerably on temperature. In their study, the degree of cross-linking may have been so high that the systems could not be elastomeric.

The tunability of the reflection notch by mechanical stress in CLCEs has been investigated under several types of deformation [6–12] and the lasing was also demonstrated for the dye-doped CLCEs [6,12,15]. Equally biaxial or uniaxial stretching of the CLCE films with the helical axis along the film thickness induced a finite shift of the reflection notch to shorter wavelengths as a result of film thinning. The blueshift of the reflection notch under equibiaxial stretching occurred without losing the reflection selectivity [6,15], while that under uniaxial stretching accompanied a considerable distortion of the regular helical configuration [8,10,11,16]. The distortion of the regular helical structure was recognized by the emergence of the reflection notch for the incident light with anticircular polarization.

Electrical actuation of CLCEs or the CLC gels, which was a CLCE swollen by LC solvent, was demonstrated experimentally [17] and considered theoretically [16,18]. The CLC gels under an electric field parallel to the helical axis exhibited a considerable degree of stretching along the field axis accompanying a finite redshift of the reflection notch.

In the present study we investigate how the temperature variation influences the photonic properties and macroscopic shape for the CLCE films with the helical axis along the film thickness. We elucidate the correlations between the thermal deformation, the orientational order of the underlying nematic structure, and the pitch of helical configuration. Further, we also examine the photonic properties for the CLCE films subjected to temperature variation but in the mechanically constrained geometry, where the thermal deformation is strictly

*Author to whom correspondence should be addressed; urayama@kit.ac.jp

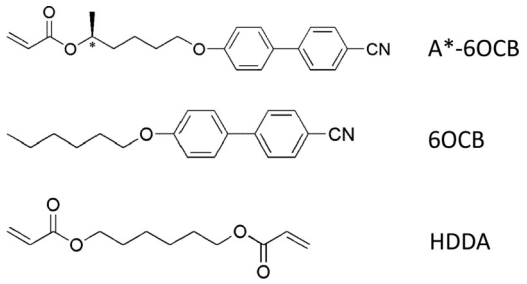

FIG. 1. Chemical structure of a monoacrylate chiral mesogen, miscible LC solvent, and cross-linker.

prohibited. It is known for nematic elastomers and gels that such mechanical frustration significantly influences the director configuration, resulting in several interesting characteristic textures [19,20]. We elucidate the influence of the mechanical constraint on the helical director configuration under temperature variation. The results in the present study provide not only an important basis for a full understanding of the physics of CLCEs but also valuable information about the tuning of the photonic properties of CLCEs using temperature variation.

II. EXPERIMENT

A. Sample preparation

The CLCE films were prepared by radical photopolymerization of the chiral mesogenic monoacylate (*A**-6OCB) and diacrylate cross-linker (HDDA) in the presence of a nonreactive achiral LC (6OCB) using IRGACURE 784 as a photoinitiator [17]. The chemical structures of *A**-6OCB, HDDA, and 6OCB are shown in Fig. 1. A molar ratio of *A**-6OCB, 6OCB, and HDDA of 1:0.82:0.07 was employed to fabricate the CLCE films. The concentration of *A**-6OCB in the mixtures governs the helical pitch in the cholesteric configuration and it was optimized so that the reflection band in the resulting CLCE films could appear in the wavelength range of visible light under temperature variation and compressive strain examined here. The photopolymerization of the reactant mixture was performed in a glass cell with a gap of 32 μm. The surfaces of the glass substrates were coated with a rubbed polyimide layer, inducing planar orientation. The mixture in the cell was annealed for 1 day at 10 °C where a monodomain Grandjean cholesteric texture with the helical axis parallel to the thickness direction was attained. After annealing, the light of a wavelength of 526 nm was irradiated at 10 °C for 30 min for polymerization. After the reaction, the glass substrates were immersed in dichloromethane and the gel films were detached from the substrates by swelling pressure. In this swelling process, the unreacted materials and unreactive solvent (6OCB) were washed out from the gel films. The gels were gradually deswollen by adding methanol to the surrounding solvent, leading to fully dried films. The thickness of the dry film was evaluated to be 25 μm at 25 °C by a DektakXT stylus profiler (Bruker).

III. MEASUREMENTS

The spectral properties were obtained using a PMA-12 spectrometer (Hamamatsu Photonics) mounted on a microscope (Nikon LV100POL). The temperature was controlled by a hot stage (Linkam TMS94). The incident white light with right- or left-circular polarization was parallel to the helical axis of the CLCE films. The CLCE films were immersed in a transparent silicone oil (nonsolvent) for lubrication between the substrate and film. The silicone oil has no effect on the transmission spectra in the wavelength range examined here. The dimensions of the rectangular films in the directions normal to the helical axis (i.e., thickness direction) and the transmission spectra were measured as a function of temperature. In the beginning of the measurements, the specimens were heated to 150 °C in the high-temperature isotropic state.

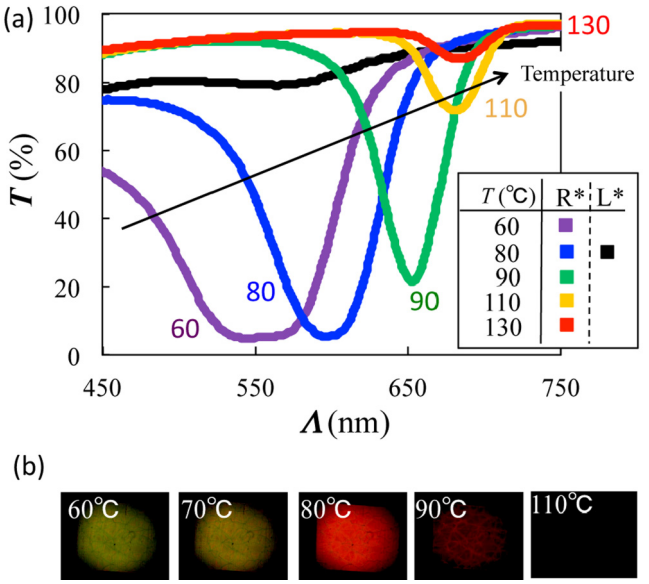

FIG. 2. (Color online) (a) Transmission spectra of the CLCE film in unconstrained geometry as a function of temperature for the incident light with right- or left-circular polarization (*R** and *L**, respectively). (b) Color of reflected light for *R** from the CLCE film at each temperature.

For the measurements in a mechanically constrained geometry, the film specimens, which were sandwiched by the transparent glass substrates, were compressed along the helical axis at 70 °C in the cholesteric state by placing a weight upon the glass cells. Thereafter the upper and bottom substrates were glued to maintain the compressed state. Silcone oil was coated on the glass substrates for lubrication. The imposed compressive strain along the thickness direction was evaluated to be 0.15 from the dimensional changes in the two directions normal to the compression using a condition of volume conservation before and after deformation.

IV. RESULTS AND DISCUSSION

A. Temperature variation in the unconstrained geometry

Figure 2(a) illustrates the transmission spectra for the incident light with right-circular polarization (designated as *R**) as a function of temperature. The transmittance for *R** exhibits a considerable reduction in a finite range of wavelength Λ, whereas that for the incident light with left-circular polarization (designated as *L**) does not, although the

data for L^* at temperatures excepting 80 °C are not shown in the figure. This feature confirms the selective reflection of the specimens for R^* in the corresponding Λ range. The central wavelength in the reflection notch Λ_R is related to the pitch of helical configuration p_H as [21]

$$\Lambda_R = p_H \left(\frac{n_o^2 + n_e^2}{2} \right)^{1/2}, \quad (1)$$

where n_o and n_e are the ordinary and extraordinary refractive indices of the underlying nematic structure. The notch of the selective reflection is strongly dependent on T and it is characterized by three parameters: Λ_R, the value of the minimum transmission $T_{\min}$, and the full width at half minimum $\Delta\Lambda$. Figures 3(a)–3(c) display the T dependence of each parameter. Each parameter depends considerably on T in the T range between the isotropic-cholesteric phase transition temperature ($T_{CI} \approx 110$ °C) and the glass transition temperature ($T_g \approx 59$ °C). The temperatures T_{CI} and T_g were evaluated by observation by a polarizing optical microscope and differential scanning calorimetry, respectively. In the range of $T_g < T < T_{CI}$, as T increases, Λ_R shifts to a higher Λ region (i.e., p_H increases) and $T_{\min}$ increases. The increases in p_H and $T_{\min}$ result from a reduction in orientational order in the underlying nematic structure S. The reduction in S upon heating is reflected in a decrease in $\Delta\Lambda$ [Fig. 3(c)], because $\Delta\Lambda/\Lambda_R$ is proportional to the optical anisotropy ($\Delta n = n_o - n_e$) of the birefringent sublayers, $\Delta\Lambda/\Lambda_R \propto \Delta n \propto S$ [22]. The redshift of the reflection notch upon heating is also recognized by a change in the color of the reflected light, which is shown in Fig. 2(b).

A finite reflection notch is observed at temperatures above T_{CI}(≈110 °C). It is generally known for LCEs prepared in the LC state that non-negligible orientational order is left at high temperatures above the transition temperature and the truly isotropic random state cannot be attained [23]. The finite reflection notch originates from the residual orientational order.

Figure 4 illustrates the macroscopic dimensional change of each specimen under temperature variation. The dimension in each direction $\lambda_i (i = x, y,$ or $z)$ is reduced by that at 130 °C in the high-temperature isotropic state. The dimensional changes in the x and y directions normal to the helical axis (z direction) are identical within the experimental error, although the data in the y direction are not shown here. The principal ratio λ_z along the helical axis is calculated using the condition of volume conservation, i.e., $\lambda_x \lambda_y \lambda_z = 1$. As T decreases, the specimens expand equivalently in the directions normal to the helical axis in the cholesteric state of $T < T_{CI}$. The dimensions become constant in the glassy state of $T < T_g$ and λ_x reaches approximately 1.1. A similar type of thermal deformation of the CLCEs was reported earlier [11,13].

Figure 5 shows the relation between the position of the reflection notch and the film dimension along the helical axis (i.e., film thickness) in the cholesteric state of $T_g < T < T_{CI}$. The data points are approximated by a straight line with an intercept of nearly zero. This linear relation indicates that the helical pitch varies in an affine manner with the film thickness under temperature variation in the unconstrained geometry.

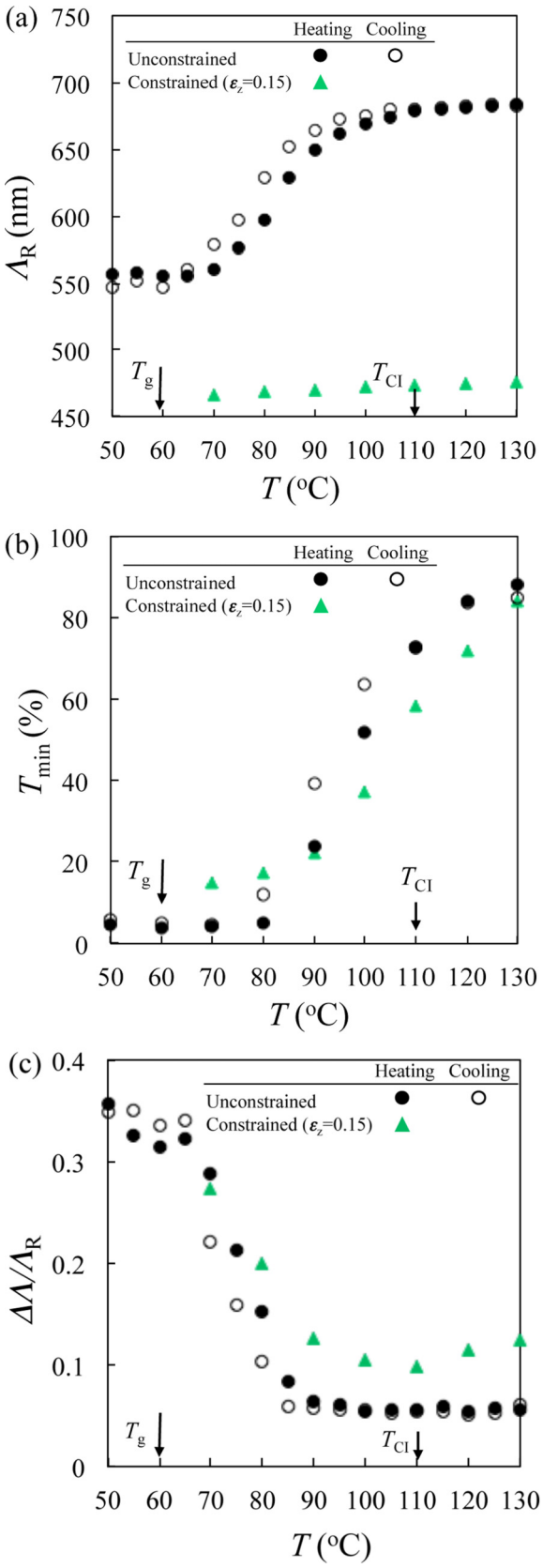

FIG. 3. (Color online) (a) Central wavelength (Λ_R), (b) minimum transmission of the reflection band $T_{\min}$, and (c) full width at half minimum ($\Delta\Lambda$) reduced by Λ_R as a function of temperature in the unconstrained and constrained geometries with a compressive strain of $\varepsilon_z = 0.15$.

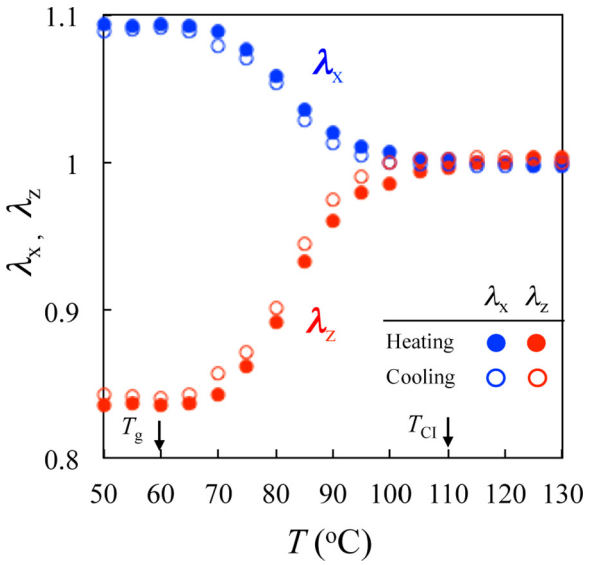

FIG. 4. (Color online) Macroscopic dimensions of the CLCE film as a function of temperature. The dimensions in the directions normal (x) and parallel (z) to the helical axis are reduced by those in the high-temperature isotropic state at 130 °C.

The macroscopic deformation is driven by a change in orientational order in the underlying nematic structure S. Figure 6 displays λ_x as a function of $\Delta\Lambda/\Lambda_R$, which is proportional to S. The data of λ_x and $\Delta\Lambda/\Lambda_R$ in the range of $T_g \leqslant T \leqslant T_{CI}$ in Figs. 3(c) and 4 are employed in the figure. The length in the direction normal to the helical axis increases with an increase in $\Delta\Lambda/\Lambda_R$, although it starts to level off at $\Delta\Lambda/\Lambda_R \approx 0.3$. The data in the level-off regime of $\Delta\Lambda/\Lambda_R > 0.3$ correspond to those at temperatures near $T_g(T_g \leqslant T \leqslant T_g + 10\,^\circ\mathrm{C})$. In the vicinity of T_g, an increase in $\Delta\Lambda/\Lambda_R$ leads to no appreciable deformation, which will be due to the effect of the glass transition.

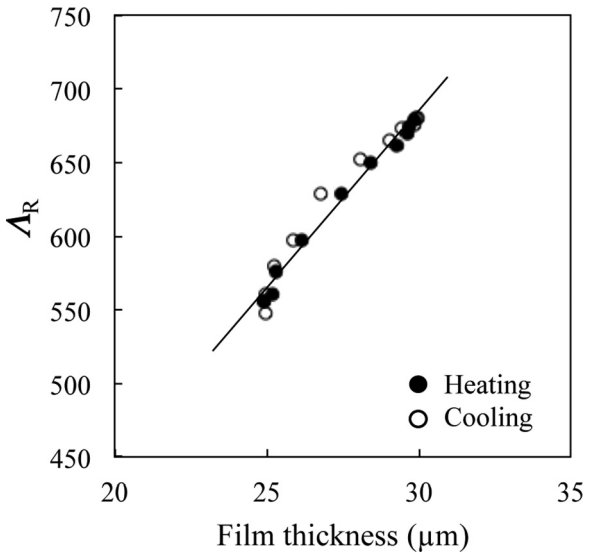

FIG. 5. Relation between the central wavelength of the reflection band Λ_R and film thickness.

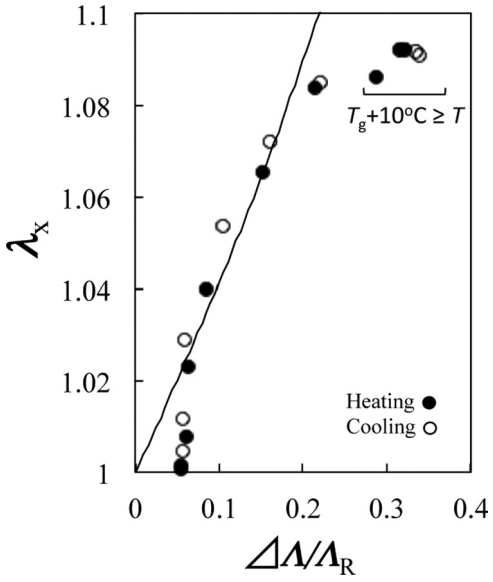

FIG. 6. Relation between λ_x and $\Delta\Lambda/\Lambda_R$ for the CLCE film in the range $T_g \leqslant T \leqslant T_{CI}$. The solid line represents the fitted result of Eq. (3) assuming $S_B = a\Delta\Lambda/\Lambda_R$ with $a = 1.55$ for the data, excepting those near T_g.

The anisotropic Gaussian chain model for LCEs proposed by Warner and Terentjev correlates the anisotropy of the dimensions of network strand with the macroscopic distortion in the CLCEs [1]

$$r = 2\lambda_x^6 - 1, \tag{2}$$

where r is a parameter for the anisotropy of the chain dimensions, i.e., the ratio of the average step lengths parallel and normal to the director. The maximum value of r is estimated to be 2.35 from Eq. (2) with the maximum value of $\lambda_x(\lambda_x = 1.09)$. The anisotropic Gaussian chain model relates r with the orientational order parameter of the network backbone S_B as $r = (1 + 2S_B)/(1 - S_B)$. The resulting relation between λ_x and S_B is expressed as

$$\lambda_x = \left[\frac{S_B + 2}{2(1 - S_B)}\right]^{1/6}. \tag{3}$$

If S_B is proportional to S, S_B is assumed as $S_B = a\Delta\Lambda/\Lambda_R$ with a proportional constant a. The solid line in Fig. 6 depicts the fitted results of Eq. (3) using a as an adjustable parameter ($a = 1.55$) for the data excepting those in the level-off regime at temperatures near $T_g(T_g \leqslant T \leqslant T_g + 10\,^\circ\mathrm{C})$. The theory describes the main feature of the experimental results in the rubbery state. A deviation of the data at $\lambda_x \approx 1$ from the theoretical line originates from a residual orientational order at $T = T_{CI}$ that is not considered in the theory. A finite deviation from the theory is also observed for the data in the high regime of $\Delta\Lambda/\Lambda_R$ that corresponds to the temperature region near $T_g(T_g \leqslant T \leqslant T_g + 10\,^\circ\mathrm{C})$. In the glass transition region, an increase in molecular order results in no significant macroscopic deformation in contrast to the rubbery regime, where the theory is applicable.

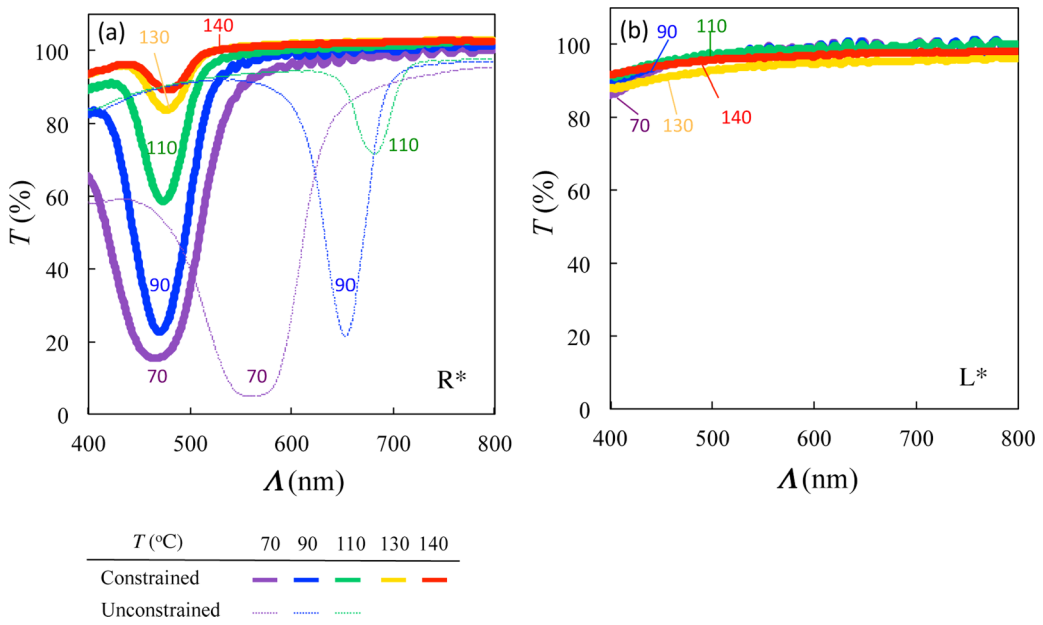

FIG. 7. (Color online) Transmission spectra of the CLCE film as a function of temperature in the constrained geometry where thermal deformation is prohibited for the incident light with (a) right- or (b) left-circular polarization (R^* or L^*, respectively). The dotted lines depict the corresponding data for R^* in the unconstrained geometry.

B. Temperature variation in the constrained geometry

The photonic properties under temperature variation are also investigated in the constrained geometry where thermal deformation is prohibited. A compressive strain of 15% along the helical axis was imposed at 70 °C in the cholesteric state and thereafter the top and bottom substrates were glued together at 70 °C to keep the strain unchanged under temperature variation. The fully mechanical constraints were confirmed by the observation of no significant dimensional change in the x and y directions under temperature variation. The imposition of the compression caused a shift of the reflection notch to the shorter wavelength regime while maintaining the selective reflection for R^*, which is shown in Fig. 7. This indicates that the compression effectively shortened the helical pitch without affecting the original helical order. The induced change in Λ_R is evaluated to be 17%, which is close to the imposed compressive strain (15%). This implies that the helical pitch varies in linear proportion to the compression, but the confirmation of the affine relation requires the data at various compressive strains, which is beyond the scope of the present study.

In this constrained geometry, the heating from T_c to T_{CI} provides a finite degree of mechanical frustration to the CLCE films, because in the unconstrained geometry, the corresponding heating induces a film thickening of approximately 10% (Fig. 4). Figures 7(a) and 7(b) display the T dependence of the transmission spectra for R^* and L^* in the constrained geometry, respectively. For comparison, the corresponding data for R^* in the unconstrained geometry are shown again in Fig. 7(a). The heating reduces the height and width of the reflection notch as in the case of unconstrained geometry, but it induces no shift of Λ_R in contrast to a considerable degree of redshift of Λ_R in the unconstrained geometry. The film remained transparent for L^* in the entire Λ range upon heating even in the constrained geometry. The T dependence of Λ_R, $T_{\min}$, and $\Delta\Lambda$ in the constrained geometry is also shown in Figs. 3(a)–3(c), respectively. These results demonstrate that the temperature variation in the constrained geometry affects the orientation order in the underlying nematic structure, but it has no effect on the helical pitch of the director configuration. This result also reveals the presence of the strong correlation between the macroscopic deformation and cholesteric configuration: The prohibition of the dimensional change results in the constraint of the variation in the cholesteric configuration.

V. SUMMARY

For the CLCEs in the unconstrained geometry, cooling induced both a redshift of the central wavelength of the reflection band Λ_R and a finite-dimensional increase in the directions normal to the axis of the helical director configuration, in the temperature range between T_g and T_{CI}. The wavelength Λ_R was in linear proportion to the film thickness under temperature variation. The thermal deformation accompanying the shift of Λ_R was driven by a change in orientational order of the underlying nematic structure S. The anisotropic Gaussian network model explains the relation between the macroscopic strain and S. Even at temperatures of $T > T_{CI}$, a finite reflection notch was observed as non-negligible orientation order due to the cross-linking in the LC state.

The strong correlation between the film thickness and the pitch of helical director configuration was also demonstrated by the CLCEs subjected to temperature variation in the constrained geometry where no thermal deformation was allowed: Temperature variation influenced the orientational order of underlying nematic structure as in the case of unconstrained geometry, but it caused no shift of Λ_R.

ACKNOWLEDGMENTS

The authors thank Daisuke Itakura for his support in the preliminary experiments. This work was partly supported by a Grant-in-Aid for Challenging Exploratory Research (Grant No. 26620179) from the Japan Society of Promotion Science and by the Eno Science Foundation.

[1] M. Warner and E. M. Terentjev, *Liquid Crystal Elastomers* (Clarendon, London, 2007).
[2] F. Brommel, D. Kramer, and H. Finkelmann, Adv. Polym. Sci. **250**, 1 (2012).
[3] S.-T. Wu and D.-K. Yang, *Reflective Liquid Crystal Displays* (Wiley, New York, 2001).
[4] M. Mitov, Adv. Mater. **24**, 6260 (2012).
[5] H. Coles and S. Morris, Nat. Photon. **4**, 676 (2010).
[6] H. Finkelmann, S. T. Kim, A. Munoz, P. Palffy-Muhoray, and B. Taheri, Adv. Mater. **13**, 1069 (2001).
[7] J. Schmidtke, W. Stille, H. Finkelmann, and S. T. Kim, Adv. Mater. **14**, 746 (2002).
[8] P. Cicuta, A. R. Tajbakhsh, and E. M. Terentjev, Phys. Rev. E **65**, 051704 (2002).
[9] M. Warner, E. M. Terentjev, R. B. Meyer, and Y. Mao, Phys. Rev. Lett. **85**, 2320 (2000).
[10] P. Cicuta, A. R. Tajbakhsh, and E. M. Terentjev, Phys. Rev. E **70**, 011703 (2004).
[11] C. Bourgerette, B. Chen, H. Finkelmann, M. Mitov, J. Schmidtke, and W. Stille, Macromolecules **39**, 8163 (2006).
[12] F. Serra, M. A. Matranga, Y. Ji, and E. M. Terentjev, Opt. Express **18**, 575 (2010).
[13] S. T. Kim and H. Finkelmann, Macromol. Rapid Commun. **22**, 429 (2001).
[14] G. Maxein, S. Mayer, and R. Zentel, Macromolecules **32**, 5747 (1999).
[15] J. Schmidtke, S. Kniesel, and H. Finkelmann, Macromolecules **38**, 1357 (2005).
[16] Y. Mao, E. M. Terentjev, and M. Warner, Phys. Rev. E **64**, 041803 (2001).
[17] Y. Fuchigami, T. Takigawa, and K. Urayama, ACS Macro Lett. **3**, 813 (2014).
[18] A. M. Menzel and H. R. Brand, Phys. Rev. E **75**, 011707 (2007).
[19] G. Skacej and C. Zannoni, Eur. Phys. J. E **20**, 289 (2006).
[20] R. Verduzco, G. N. Meng, J. A. Kornfield, and R. B. Meyer, Phys. Rev. Lett. **96**, 147802 (2006).
[21] H. de Vries, Acta Crystallogr. **4**, 219 (1951).
[22] P. G. de Gennes and J. Prost, *The Physics of Liquid Crystals*, 2nd ed. (Oxford University Press, New York, 1993).
[23] A. Lebar, G. Cordoyiannis, Z. Kutnjak, and B. Zalar, Adv. Polym. Sci. **250**, 147 (2012).